TISSUE REGENERATION

Defective cholesterol clearance limits remyelination in the aged central nervous system

Ludovico Cantuti-Castelvetri,[1,2,3,4]* Dirk Fitzner,[1,5]* Mar Bosch-Queralt,[1,2,3,4] Marie-Theres Weil,[1,6] Minhui Su,[1,2,3,4] Paromita Sen,[1] Torben Ruhwedel,[7] Miso Mitkovski,[8] George Trendelenburg,[5] Dieter Lütjohann,[9] Wiebke Möbius,[6,7] Mikael Simons[1,2,3,4]†

Age-associated decline in regeneration capacity limits the restoration of nervous system functionality after injury. In a model for demyelination, we found that old mice fail to resolve the inflammatory response initiated after myelin damage. Aged phagocytes accumulated excessive amounts of myelin debris, which triggered cholesterol crystal formation and phagolysosomal membrane rupture and stimulated inflammasomes. Myelin debris clearance required cholesterol transporters, including apolipoprotein E. Stimulation of reverse cholesterol transport was sufficient to restore the capacity of old mice to remyelinate lesioned tissue. Thus, cholesterol-rich myelin debris can overwhelm the efflux capacity of phagocytes, resulting in a phase transition of cholesterol into crystals and thereby inducing a maladaptive immune response that impedes tissue regeneration.

Remyelination restores rapid transmission of nerve impulses and axonal function in the central nervous system (CNS) of patients with demyelinating diseases such as multiple sclerosis (MS). Although remyelination can occur in MS, age-associated decline in myelin repair contributes to chronic progressive disease and disability (*1*). Thus, understanding the cause of and preventing this decline are key goals in regenerative medicine (*2*–*4*). So far, epigenetic changes within aging oligodendrocyte progenitor cells and declines in phagocytic capacity of aged blood-derived monocytes have been identified as possible mechanisms (*5*, *6*). We implemented a toxin-induced model, in which a single injection of lysolecithin (lysophosphatidylcholine) induces a focal demyelinating lesion in the white matter of the brain or spinal cord of mice. In lesioned animals, demyelination is complete within 4 days, followed by a repair process that is maximal between 14 and 21 days postinjection (dpi) and requires rapid clearance of damaged myelin for regeneration to occur (*7*).

[1]Max Planck Institute of Experimental Medicine, 37075 Göttingen, Germany. [2]Munich Cluster for Systems Neurology (SyNergy), 81377 Munich, Germany. [3]Institute of Neuronal Cell Biology, Technical University Munich, 80805 Munich, Germany. [4]German Center for Neurodegenerative Disease (DZNE), 81377 Munich, Germany. [5]Department of Neurology, University of Göttingen Medical Center, 37075 Göttingen, Germany. [6]Center for Nanoscale Microscopy and Molecular Physiology of the Brain (CNMPB), 37075 Göttingen, Germany. [7]Department of Neurogenetics, Max Planck Institute of Experimental Medicine, 37075 Göttingen, Germany. [8]Light Microscopy Facility, Max Planck Institute of Experimental Medicine, 37075 Göttingen Germany. [9]Institute for Clinical Chemistry and Clinical Pharmacology, University of Bonn, 53127 Bonn, Germany.
*These authors contributed equally to this work.
†Corresponding author. Email: msimons@gwdg.de

We induced focal demyelinating lesions in the corpus callosum of young (3 months) and old (12 months) mice by lysolecithin injections. Lesions were of similar size at 4 dpi but not at 14 dpi, confirming the poor regenerative capacity of old mice (Fig. 1, A to C, and fig. S1, A to E). Sustained immune infiltration, as determined by IBA1-positive and MAC2-positive cells, was detected in old mice at 14 dpi (Fig. 1, A and E, and fig. S1G). Myelin debris accumulation within lysosomes of phagocytes (Fig. 1, D and F) and numerous foam cells harboring lipid droplets and needle-shaped cholesterol crystals—a typical hallmark of cholesterol overloading—were found in old mice (Fig. 1, G and H, and fig. S2G). Moreover, by a combination of laser reflection and fluorescence confocal microscopy (reflection microscopy) we confirmed the increase of crystal deposition in spinal cord lesions of old mice (Fig. 1, I and J). Crystals were similarly observed in two other models of myelin injury (fig. S2).

Toxic overload of cholesterol drives the formation of foamy macrophages and maladaptive immune responses in atherosclerosis. We hypothesized that the accumulation of cholesterol, the major component of myelin, may overwhelm the cholesterol transport capacity of phagocytes, thereby forming a bottleneck for successful repair in the aged CNS. Because cholesterol cannot be broken down, it must be transferred from the phagocytes back to the extracellular space via the transporters ABCA1 and ABCG1 [adenosine triphosphate–binding cassette (ABC) A1 and G1] in the plasma membrane where it binds high-density lipoprotein particles [e.g., apolipoprotein E (APOE)] (*8*). Real-time quantitative reverse transcription polymerase chain reaction (PCR) analyses revealed that the expression of *ApoE*, *Abca1*, and *Abcg1* was reduced in 4-dpi lesions of old mice compared with young mice (Fig. 1, K to M, and fig. S3). Oxysterols (hydroxylated cholesterol metabolites) such as 24*S*- and 27-hydroxycholesterol are endogenous ligands for the liver X receptor (LXR), thereby controlling the expression of genes involved in cholesterol efflux in cholesterol-loaded cells (*9*). Relative amounts of 24*S*-hydroxycholesterol did not differ in lesions of young and old animals, but 27-hydroxycholesterol levels were reduced in lesions of old mice (fig. S3). One possible explanation for lesion restitution failure in old mice is the inability to clear excessive myelin-derived cholesterol from phagocytes. Thus, we examined whether the LXR agonist GW3965 (*10*) improve lesion recovery in old mice by inducing the expression of genes involved in lipid efflux, such as *Abca1*, *Abcg1*, and *ApoE* (fig. S3). GW3965 led to markedly improved lesion regeneration in old mice, with a reduction in the number of IBA1-positive and MAC2-positive phagocytes (Fig. 1, A to C). In addition, the number of phagocytes containing myelin debris, the number of foam cells, and the amount of cholesterol crystals were reduced by treatment with GW3965 (Fig. 1, A to J).

Because accumulation of cholesterol in phagocytes may pose a barrier for successful tissue regeneration, we analyzed the regenerative capacity of mouse mutants lacking central factors of the reverse cholesterol transport pathway. We induced demyelinating lesions in 3-month-old NR1H3 (or LXRα) knockout (KO) mice and observed, as in aged wild-type (WT) mice, impaired lesion restitution and sustained phagocyte infiltration at 21 dpi (fig. S4, A to C). In addition, we detected accumulation of myelin debris in lysosomes of phagocytes and crystal deposition in lesions of LXRα KO mice (fig. S4, D to G).

Next, we analyzed the role of APOE, the major CNS cholesterol carrier that supports lipid efflux from cells (*11*). We induced focal demyelination in the corpus callosum of 12-week-old APOE KO and WT control mice and quantified lesion size and recovery. Lesion size did not differ initially, at 4 dpi (fig. S4, H to J). However, when lesions were analyzed at 21 dpi, we observed impaired lesion restitution. We detected increased numbers of IBA1-positive, MAC2-positive, and major histocompatibility complex class II (MHC II)–positive phagocytes, as well as enhanced crystal deposition and myelin debris accumulation within lysosomes of phagocytes in spinal cord and corpus callosum lesions of APOE KO animals as compared with control mice (Fig. 2 and fig. S5). Because APOE has functions beyond cholesterol transport (*11*), we tested the efficacy of cyclic oligosaccharide 2-hydroxypropyl-β-cyclodextrin (HβCD), a compound that increases cholesterol efflux and solubility (*12*), and found that HβCD treatment attenuated the phenotype of APOE KO animals (Fig. 3 and fig. S6).

Together with *Abca1* and *Abcg1*, *ApoE* represents one of the major nuclear LXR–regulated genes involved in mediating cholesterol efflux from phagocytes. We thus crossbred CX3CR1CreER animals with $Abca1^{fl/fl}$ and $Abcg1^{fl/fl}$ mice to obtain microglia- and macrophage-specific double-KO mice (ABCA1 and ABCG1 KO). We observed

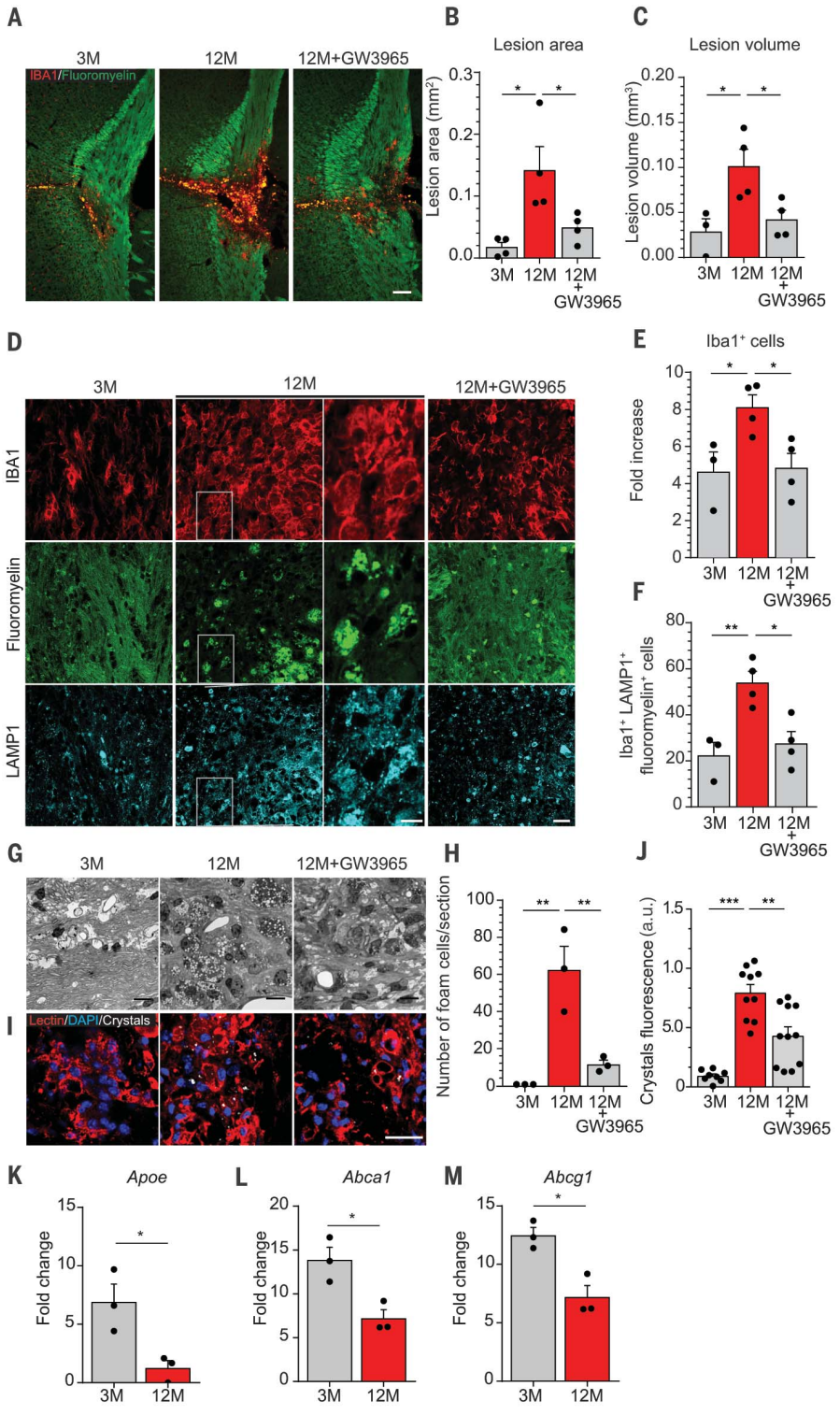

Fig. 1. Defective cholesterol clearance limits lesion regeneration in aged mice. (**A**) Images of corpus callosum lesions stained with fluoromyelin (green) and IBA1 (red) in 3-month-old (3M), 12-month-old (12M), and 12-month-old mice treated with GW3965 (12M+GW3965) at 14 dpi. Scale bar, 100 μm. (**B** and **C**) Quantification of lesion area in square millimeters, determined by luxol fast blue (LFB) staining, and in cubic millimeters, determined by fluoromyelin staining, at 14 dpi. (**D**) Confocal images of 3M, 12M, and 12M+GW3965 corpus callosum lesions showing IBA1 (red), fluoromyelin (green), and LAMP1 (blue). Scale bars, 40 μm. For 12M animals, the panels at right are magnified images of the boxed areas at left. (**E**) Change in number of IBA1$^+$ cells in corpus callosum lesions compared with the contralateral unlesioned side. (**F**) Number of IBA1$^+$, fluoromyelin$^+$, and LAMP1$^+$ cells in lesioned corpus callosum tissue at 14 dpi. (**G**) Semithin sections and (**H**) quantification of foam cells of 3M, 12M, and 12M+GW3965 corpus callosum lesions. Scale bars, 10 μm. (**I**) Reflection microscopy images of spinal cord lesions, showing crystals (white) in lectin$^+$ phagocytes (red), and (**J**) relative quantification of the fluorescence intensity of the reflected light. Scale bar, 25 μm. DAPI, 4′,6-diamidino-2-phenylindole; a.u., arbitrary units. (**K** to **M**) Quantitative PCR analysis of *Apoe*, *Abca1*, and *Abcg1* in 4-dpi lesions of 3M and 12M mice. All data are mean ± SEM (error bars); **P* < 0.05, ***P* < 0.01, ****P* < 0.001 by one-way analysis of variance (ANOVA) test, with Tukey's multiple comparison test.

an increased number of IBA1-positive and MHC II–positive phagocytes, an increase in crystal deposition, and fewer myelinated axons in 21-dpi lesions of ABCA1 and ABCG1 KO animals as compared with controls (fig. S7).

Because excessive cholesterol accumulation in phagocytes limits lesion recovery, we turned to cell culture experiments to determine the mechanisms involved. We prepared phagocytes [primary microglia or bone marrow–derived macrophages (BMDMs)] from APOE KO and WT mice and examined the phagocytic uptake of myelin debris, which did not differ in cells prepared from WT or APOE KO mice (fig. S8, A and B). Because APOE is also produced by astrocytes, we incubated cells in the presence of serum-free conditioned media prepared from either WT or APOE KO astrocytes and observed the clearance of the internalized myelin particles from phagocytes. Myelin debris persisted within lysosomes of APOE KO cells that were incubated with conditioned media from APOE KO astrocytes. Clearance could be improved by an APOE-derived mimetic peptide, ATI5261 (*13*), which contains an amphipathic α-helical motif responsible for lipid binding and cholesterol efflux (Fig. 3, E and F). Moreover, myelin debris treatment

resulted in crystal formation, which was increased in APOE KO macrophages and reduced by GW3965 treatment (fig. S8, C to G).

In atherosclerosis, cholesterol crystals can induce inflammation by phagolysosomal membrane rupture and subsequent stimulation of the caspase-1–activating NLRP3 (NALP3 or cryopyrin) inflammasome and secretion of interleukin (IL)–1 cytokines (*14*, *15*). Myelin debris treatment resulted in lysosomal permeabilization and caspase-1 cleavage in WT but not in NLRP3-deficient macrophages (Fig. 4, A to H, and fig. S9, A and B). More pronounced caspase-1 activation was observed in APOE KO as compared with WT macrophages, which was confirmed in vivo in APOE KO mice after lysolecithin injection (Fig. 4E and fig. S9C). Myelin overloading induced cell death, which resulted in DNA fragmentation [detected by TUNEL (terminal deoxynucleotidyl transferase–mediated deoxyuridine triphosphate nick end labeling) assay], was cholesterol dependent (fig. S9, D and E), and was rescued by caspase-1 inhibitors, pointing to an inflammasome-mediated pyroptotic cell death pathway (Fig. 4G and fig. S10). Thus, cholesterol derived from myelin debris can activate the NLRP3 inflammasome in macrophages when toxic levels build up intracellularly in the absence of sufficient lipoprotein carriers.

Because jamming the lysosomal system with myelin debris resulted in cholesterol crystallization and inflammasome activation, we asked whether this pathway was responsible for limiting regeneration in old mice. To examine whether increased inflammasome activation contributed to the poor recovery of old mice, we

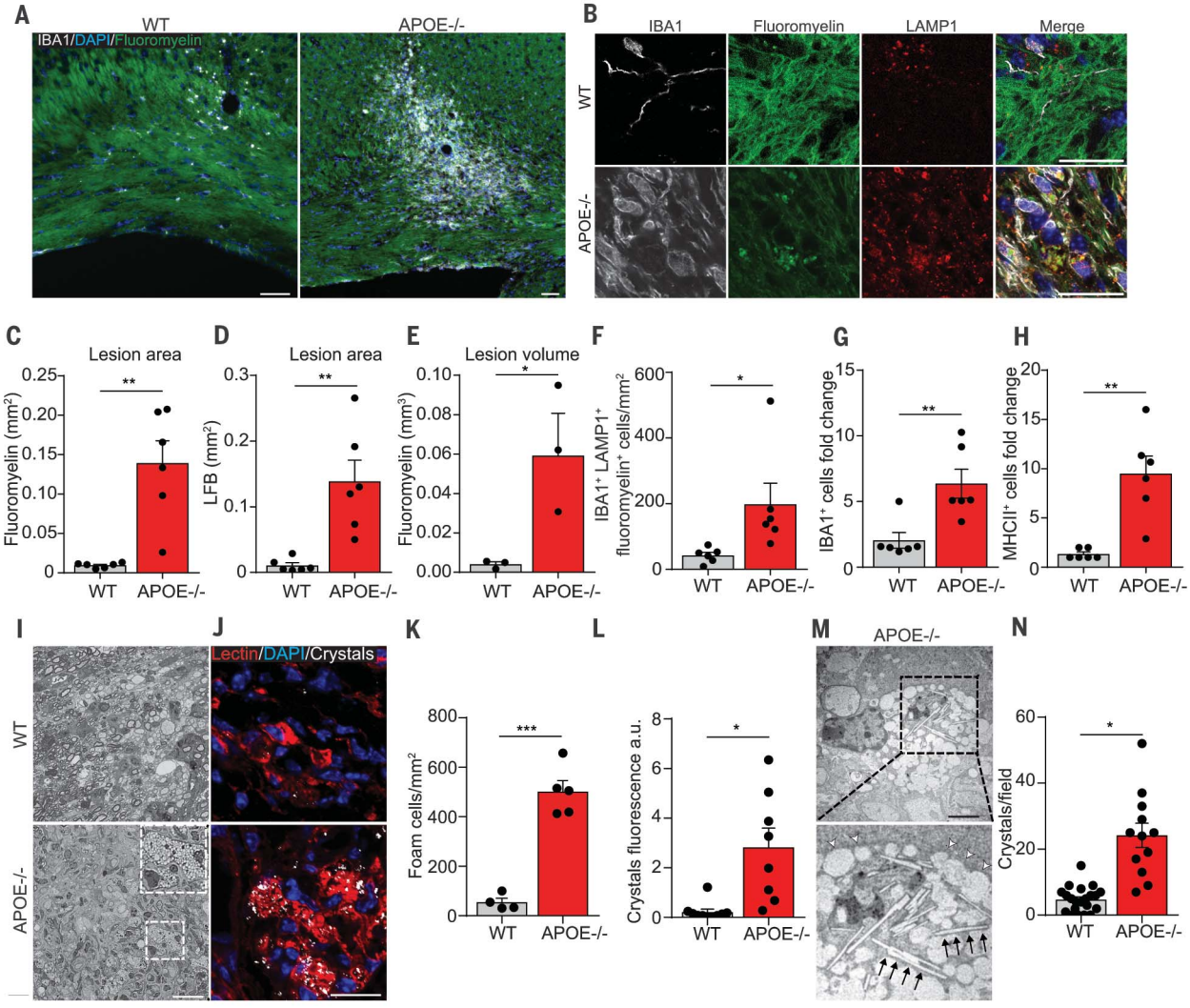

Fig. 2. APOE is required for cholesterol clearance in demyelinating lesions. (**A** and **B**) Images of corpus callosum lesions in WT and APOE$^{-/-}$ mice at 21 dpi showing fluoromyelin staining (green), IBA1 (white), DAPI (blue), and LAMP1 (red). (**C** and **D**) Quantification of lesion area in square millimeters at 21 dpi, as determined by fluoromyelin and LFB staining. (**E**) Lesion volume in cubic millimeters, as measured by fluoromyelin staining in consecutive sections. (**F**) Number of IBA1$^+$, fluoromyelin$^+$, and LAMP1$^+$ cells per square millimeters in lesions at 21 dpi. (**G** and **H**) Change in the number of IBA1$^+$ and MHC II$^+$ cells in the lesioned corpus callosum as compared with the contralateral unlesioned side. (**I**) Representative images (boxed area of bottom left panel shown at larger magnification in right corner) and (**K**) quantification of foam cells in spinal cord lesions in WT and APOE$^{-/-}$ mice at 21 dpi. (**J**) Reflection microscopy images of 21-dpi lysolecithin lesions, showing crystals (white) in lectin$^+$ phagocytes (red), and (**L**) relative quantification of the fluorescence intensity of the reflected light. (**M**) Transmission electron microscopy images of foam cells in 21-dpi lesions of APOE$^{-/-}$ mice (the boxed area is shown below at higher magnification), showing needle-like cholesterol crystals (black arrows) and lipid droplets (white arrowheads), and (**N**) relative quantification of crystals. All data are mean ± SEM (error bars); *P < 0.05, **P < 0.01, ***P < 0.001 by two-tailed Student's t test. Scale bars in (A), (B), (I), and (J), 25 μm; scale bar in (K), 2.5 μm.

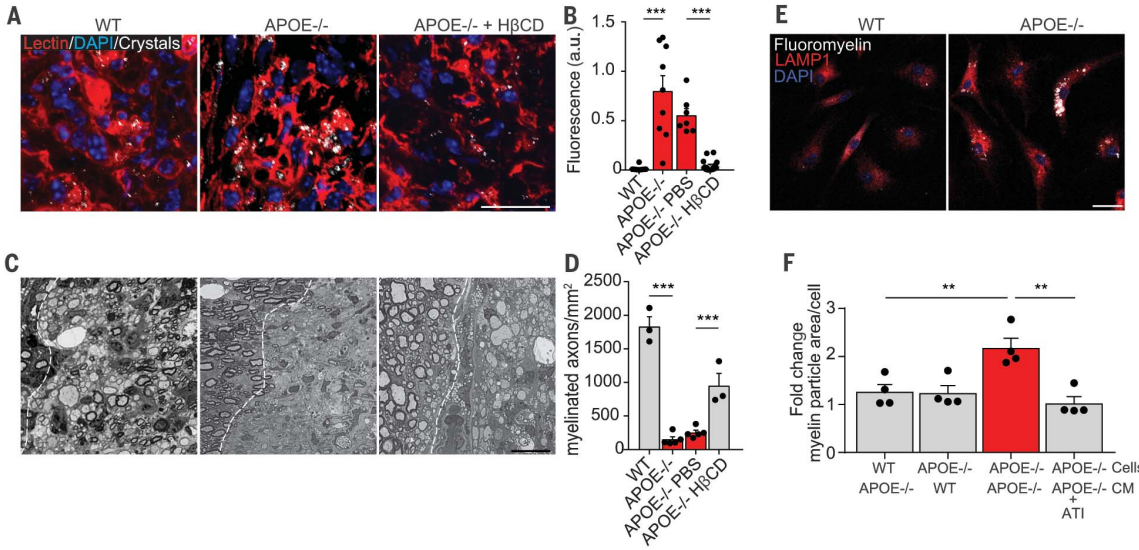

Fig. 3. Enhancing cholesterol clearance prevents lysosomal storage of myelin debris and crystal formation. (**A**) Representative images with crystals (white) and lectin^{+} phagocytes (red), and (**B**) quantification of cholesterol crystals in lysolecithin lesions of WT, APOE$^{-/-}$, and APOE$^{-/-}$ mice treated with HβCD or phosphate-buffered saline (PBS). Scale bar, 25 μm. (**C**) Representative images of methylenblue-azur II staining and (**D**) quantification of remyelination in lysolecithin lesions at 21 dpi. In (C), the edges of the lesions are identified by dashed lines. Scale bar, 25 μm. (**E**) Confocal images of primary microglial cell cultures prepared from WT or APOE$^{-/-}$ mice, treated with myelin debris and stained for LAMP1 (red), fluoromyelin (white), and DAPI (blue) at 24 hours posttreatment. Microglia from WT or APOE$^{-/-}$ mice were treated with myelin debris and subsequently transferred in media conditioned either by WT or APOE$^{-/-}$ astrocytes. APOE$^{-/-}$ microglia cells in APOE$^{-/-}$ conditioned media (CM) were additionally treated with APOE mimetic peptide (ATI). Scale bar, 25 μm. (**F**) Change in the area of myelin particles per cell as compared with WT cells in WT conditioned media. All data are mean ± SEM (error bars); $^{**}P < 0.01$, $^{***}P < 0.001$ by two-way ANOVA, with Tukey's multiple comparison test.

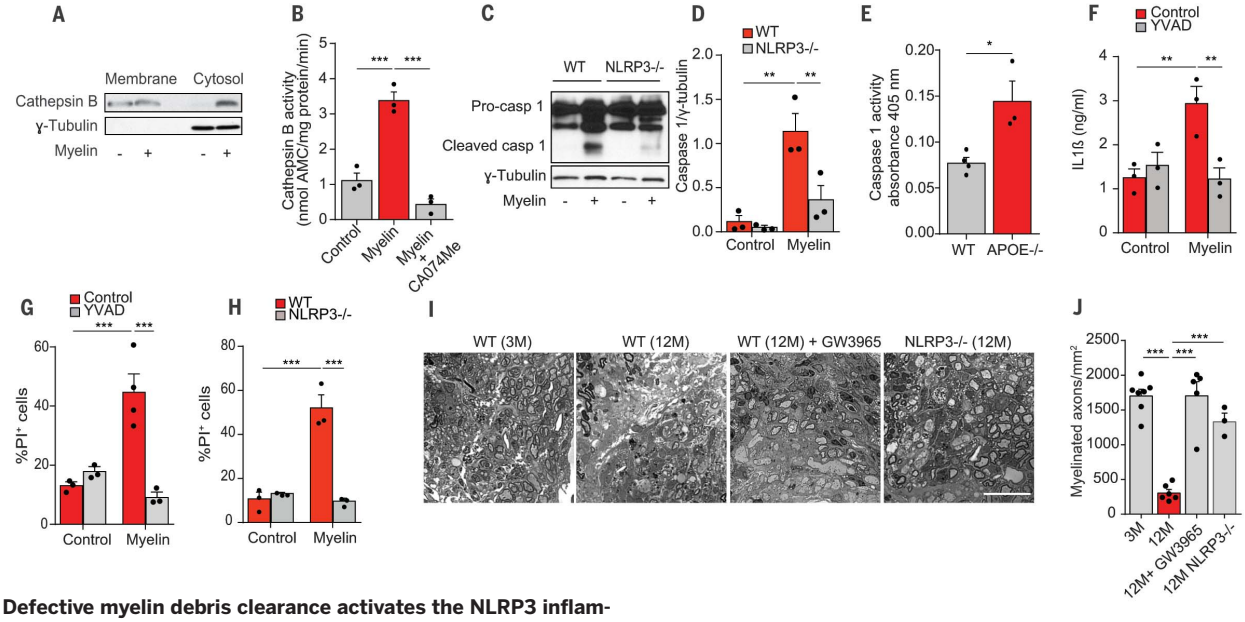

Fig. 4. Defective myelin debris clearance activates the NLRP3 inflammasome. (**A**) Immunoblot of cytosol and membrane fractions of primary BMDMs 12 hours after treatment with myelin debris for cathepsin B and γ-tubulin. (**B**) Cathepsin B activity assay of the cytosolic fraction of control macrophages 12 hours after treatment with myelin debris in the presence or absence of the cathepsin B inhibitor CA074me (10 μM). AMC, 7-amino-4-methylcoumarin. (**C** and **D**) Immunoblot and quantification of the active subunit of caspase 1 (p20) after myelin debris treatment of WT or NLRP3$^{-/-}$ BMDMs. The intensity of the p20 band was normalized to γ-tubulin. (**E**) Caspase 1 activity in lysates from lysolecithin lesions of WT and APOE$^{-/-}$ mice at 21 dpi. (**F**) Enzyme-linked immunosorbent assay for IL-1β release in WT BMDMs, after treatment with myelin debris with or without YVAD. (**G**) Quantification of the percentage of dead cells [propidium iodide–positive (PI^{+})] after myelin debris treatment (12 hours) in the presence or absence of a caspase-1 inhibitor (YVAD). (**H**) Quantification of PI^{+} cells after treatment of WT and NLRP3$^{-/-}$ BMDMs with myelin debris for 12 hours. (**I**) Methylenblue-azur II staining of remyelinating lesions in the spinal cord of 3M, 12M, GW3965-treated 12M, and 12M NLRP3$^{-/-}$ mice and (**J**) relative quantification of myelinated fibers. All data are mean ± SEM (error bars); $^{*}P < 0.05$, $^{**}P < 0.01$, $^{***}P < 0.001$ by one-way ANOVA test, with Tukey's multiple comparison test and two-tailed Student's *t* test (E). Scale bar in (I), 25 μm.

analyzed spinal cord lesions of aged WT and NLRP3-deficient mice. As in GW3965-treated old animals (Fig. 4, I and J), we found significantly improved remyelination in aged NLRP3-deficient mice as compared with aged WT mice at 21 dpi. Thus, inflammasome activation, possibly downstream of cholesterol accumulation, drives a maladaptive immune response that hampers inflammation resolution and repair in aged mice.

Self-resolving inflammation is essential for a proper restorative process after tissue damage, whereas uncontrolled inflammation can leave lasting marks that permanently alter tissue homeostasis (*16*). We made the surprising discovery that the self-limiting inflammatory response, which is necessary to initiate a regenerative process, is maladaptive in the CNS of aged mice. It appears that the inability of aged phagocytes to clear the enormous amounts of cholesterol that are released from myelin after myelin breakdown in demyelinating diseases results in a phase transition of free cholesterol into crystals, inducing lysosomal rupture and inflammasome stimulation, consistent with the beneficial effects of nuclear receptor agonists in remyelination (*17*, *18*). The unexpected link between lipid metabolisms and tissue regeneration provides opportunities for the development of regenerative medicines for remyelination and for improving functional recovery after CNS injury (*19*).

REFERENCES AND NOTES

1. P. Patrikios *et al*., *Brain* **129**, 3165–3172 (2006).
2. F. J. Najm *et al*., *Nature* **522**, 216–220 (2015).
3. F. Mei *et al*., *Nat. Med.* **20**, 954–960 (2014).
4. V. A. Deshmukh *et al*., *Nature* **502**, 327–332 (2013).
5. J. M. Ruckh *et al*., *Cell Stem Cell* **10**, 96–103 (2012).
6. S. Shen *et al*., *Nat. Neurosci.* **11**, 1024–1034 (2008).
7. V. E. Miron *et al*., *Nat. Neurosci.* **16**, 1211–1218 (2013).
8. K. J. Moore, I. Tabas, *Cell* **145**, 341–355 (2011).
9. X. Fu *et al*., *J. Biol. Chem.* **276**, 38378–38387 (2001).
10. C. Hong, P. Tontonoz, *Nat. Rev. Drug Discov.* **13**, 433–444 (2014).
11. R. W. Mahley, *Science* **240**, 622–630 (1988).
12. S. Zimmer *et al*., *Sci. Transl. Med.* **8**, 333ra50 (2016).
13. A. Hafiane, J. K. Bielicki, J. O. Johansson, J. Genest, *Biochim. Biophys. Acta* **1841**, 1498–1512 (2014).
14. P. Duewell *et al*., *Nature* **464**, 1357–1361 (2010).
15. K. Rajamäki *et al*., *PLOS ONE* **5**, e11765 (2010).
16. A. Aguzzi, B. A. Barres, M. L. Bennett, *Science* **339**, 156–161 (2013).
17. J. K. Huang *et al*., *Nat. Neurosci.* **14**, 45–53 (2011).
18. D. Meffre *et al*., *Proc. Natl. Acad. Sci. U.S.A.* **112**, 7587–7592 (2015).
19. F. Bei *et al*., *Cell* **164**, 219–232 (2016).

ACKNOWLEDGMENTS

We thank L. Vaculčiaková for help with the calculations of three-dimensional reconstructions and A. Kerksiek for technical assistance. This work was supported by a European Research Council (ERC) Consolidator Grant (M.S.) and grants from the German Research Foundation (DFG) (SI 746/9-1,10-1, SPP1757, TRR128, and TRR43), the Klaus Tschira Stiftung, the Adelson Foundation, Excellence Cluster for Systems Neurology (SyNergy), and Excellence Cluster for Nanoscale Microscopy and Molecular Physiology of the Brain (CNMPB). W.M. is supported by an ERC grant to K.-A. Nave. M.B.-Q. is supported by a Boehringer Ingelheim stipend. All data are presented in the main text and supplementary materials.

SUPPLEMENTARY MATERIALS

www.sciencemag.org/content/359/6376/684/suppl/DC1
Materials and Methods
Figs. S1 to S10
References (*20*–*29*)

10 April 2017; resubmitted 5 November 2017
Accepted 11 December 2017
Published online 4 January 2018
10.1126/science.aan4183

Science

Defective cholesterol clearance limits remyelination in the aged central nervous system

Ludovico Cantuti-Castelvetri, Dirk Fitzner, Mar Bosch-Queralt, Marie-Theres Weil, Minhui Su, Paromita Sen, Torben Ruhwedel, Miso Mitkovski, George Trendelenburg, Dieter Lütjohann, Wiebke Möbius and Mikael Simons

Science **359** (6376), 684-688.
DOI: 10.1126/science.aan4183originally published online January 4, 2018

Keeping cholesterol at bay

A decline in tissue repair is a universal hallmark of aging. The failure to regenerate myelin sheaths in multiple sclerosis lesions contributes to chronic progressive disease and disability. Understanding the cause and preventing this failure is a key goal in regenerative medicine. Cantuti-Castelvetri *et al.* report that the self-limiting inflammatory response, which is necessary for remyelination to occur, is maladaptive in the central nervous system (CNS) of old mice (see the Perspective by Chen and Popko). Cholesterol-rich myelin debris overwhelmed the efflux capacity of phagocytes, resulting in a transition of free cholesterol into crystals, thereby inducing lysosomal rupture and inflammasome stimulation. Thus, drugs being developed to promote cholesterol clearance in human atherosclerosis lesions may also be good candidates for regenerative medicine in the CNS.

Science, this issue p. 684; see also p. 635